Supporting Information

Inspired by Wet Adhesion Behavior of Mussels to Construct Robust Cathode Protection Layer towards High-Performance Aqueous Zinc-ion Batteries

Qianzhi Gou[a,b*#], Sida Zhang[b#], Huaping Mei[a], Chang Liu[c], Haoran Luo[b], Kaixin Wang[b], Yuzhi Hu[b], Bingye Song[a*], Yujie Zheng[b], Mingtao Qiao[c*], Meng Li[b*]

a. School of Building Services Science and Engineering, Xi'an University of Architecture and Technology, Xi'an, 710055, China

b. National Innovation Center for Industry-Education Integration of Energy Storage, MOE Key Laboratory of Low-grade Energy Utilization Technologies and Systems, CQU-NUS Renewable Energy Materials & Devices Joint Laboratory, College of Energy & Power Engineering, Chongqing University, Chongqing 400044, China.

c. College of Materials Science and Engineering, Xi'an University of Architecture and Technology, Xi'an, 710055, China

Corresponding author: gqz813@xauat.edu.cn, bysong@xauat.edu.cn, mtqiao@xauat.edu.cn, limeng@cqu.edu.cn

# These authors contribute equally to this work

Experimental section

Materials

Potassium permanganate ($KMnO_4$, AR), manganese sulfate ($MnSO_4$, AR), zinc sulfate heptahydrate ($ZnSO_4•7H_2O$, AR) were purchased from MACKLIN company, and all the chemicals were used as received without further purification. Concentrated hydrochloric acid were obtained from Chuandong chemical company. Tris-buffer aqueous solution (pH=8.5) was obtained from the Aladdin company. The de-ionized (DI) water was obtained from an ultra-pure purification system.

Synthesis of pure α-MnO_2 (MO) sample.

The MnO_2 nanotubes were prepared *via* a facile hydrothermal method with a minor revision. Firstly, 0.675 g $KMnO_4$ and 1.5 ml concentrated HCl were added to 60 ml de-ionized (DI) water under stirring for 30 min. Afterwards, the obtained purple solution was transferred into a Teflon-lined autoclave and heated at 160 °C for 12 h. Finally, the product was collected after

being filtered, washed with DI water and ethanol, and dried at 70°C for 12 h.

Synthesis of polydopamine coated α-MnO_2 (PDMO) sample.

Typically, 300 mg of MO nanotubes were dispersed in 40 mL Tris-buffer aqueous solution (pH=8.5) to form a homogeneous solution. Then, 100 mg of dopamine hydrochloride powder was slowly added into the mixture after stirring for 8 h. Finally, the black products were washed by DI water a for three times, and then dried at 70℃ for 12 h, thereby obtaining the final PDMO sample.

Preparation of both cathode materials.

Both cathode materials are composed of MO/PDMO sample, conductive super-P and PVDF at a mass ratio of 7:2:1 in N-methyl pyrrolidone solvent. Afterwards, the slurry mixture was coated on the Ti foil (thickness=0.03 mm), and then dried in 80℃ overnight in a vacuum oven. Finally, the overall Ti foil containing active materials were cut into discs of 14 mm diameter (mass loading of 1.0-1.5 mg cm^{-2}).

Materials Characterization

Morphology and microstructure of the as-obtained samples were characterized *via* scanning electron microscopy (SEM, Zeiss Auriga SEM-FIB) and transmission electron microscopy (TEM, FEI Talos F200S G2). The phase structures of both powder samples were analyzed on the Bruker D2 Phaser X-ray diffractometer (XRD) with Cu-Kα radiation (λ=1.54178 Å) ranging from 10 to 80°. X-ray photoelectron spectroscopy (XPS) technique with an Al Kα radiation source was utilized to determine the information of elemental composition and valence state of for the samples. Raman spectra for both samples were measured via Raman spectroscopy (Thermo-Fisher Scientific, excitation from an argon-ion laser excitation wavelength, 532 nm), and Fourier transform infrared spectra (FTIR) obtained from the Nicolet IS10 spectrometer was utilized to obtain the information of functional groups. The Barrett-Joyner-Halenda (BJH) and Brunauer- Emmett-Teller (BET) model was utilized to measure the pore size distribution and the specific surface area (SBET) of various samples, respectively. Thermogravimetric analysis (TGA) of PDMO samples was performed with at temperature ramp of 10 °C min^{-1} under air flow.

Electrochemical Measurements

The electrochemical performance of both cathode materials was evaluated using a standard CR2032 coin-type cells which were assembled in air condition. The as-obtained electrode, zinc metal plate, glass microfiber (Whatman, GF/D), and 2 M $ZnSO_4$ aqueous solution with 0.2 M $MnSO_4$ additive were applied as cathode, anode, separator, and electrolyte, respectively. The cyclic voltammogram (CV) curves and electrochemical impedance spectra (EIS) tests were tested in coin cells via Bio-Logic electrochemical workstation. Moreover, the galvanostatic charge and discharge tests (GCD) at various current densities with a potential window ranging from 0.8 to 1.8 V vs Zn/Zn^{2+} were performed using the NEWARE battery test system. All the tests were performed at room temperature. Finally, the galvanostatic intermittent titration technique (GITT) tests were conducted on a LAND battery test system.

Theoretical Calculations

The first-principles calculations within the framework of Density Functional Theory (DFT) were conducted to compare the H_2O molecule adsorption properties onto the MnO_2 and DA substrate via employing the Vienna *Ab initial* Simulation Package (VASP).[1-3] We employed the projector-augmented-wave (PAW) pseudopotentials and Perdew-Burke-Ernzerhof (PBE) exchange and correlation functionals.[2, 4] The plane-wave basis cutoff energy of 520 eV was used for the self-consistent field method with an electronic energy convergence of 1×10^{-5} eV/atom, and the 3×3×1 k-point samplings were applied within the Γ center Monkhorst-Pack scheme. For the lattice constants optimization, the remanent Hellmann-Feynman forces are less than 0.01 eV/Å. In addition, the DFT+U method was used to correct the strongly correlated interaction and its parameters, and the value of U is 3.9 eV.[5, 6] Finally, the calculations of the electrostatic potential (ESP) on the molecular surface were performed via Multiwfn, and all visualizations were implemented by VMD software.[7, 8]

Figure section:

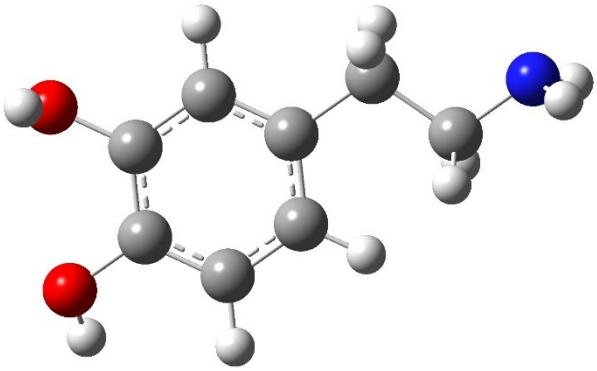

Figure S1 Molecular model of dopamine (red: O atom, white: H atom, blue: N atom, gray: C atom).

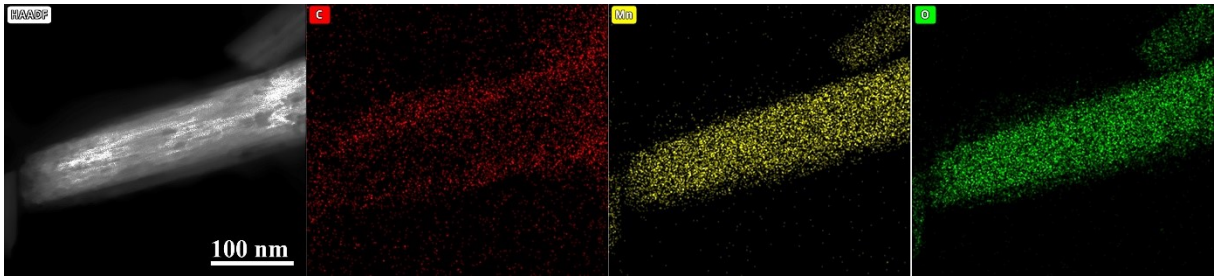

Figure S2 EDX mapping of PDMO nanotube obtained from TEM analysis.

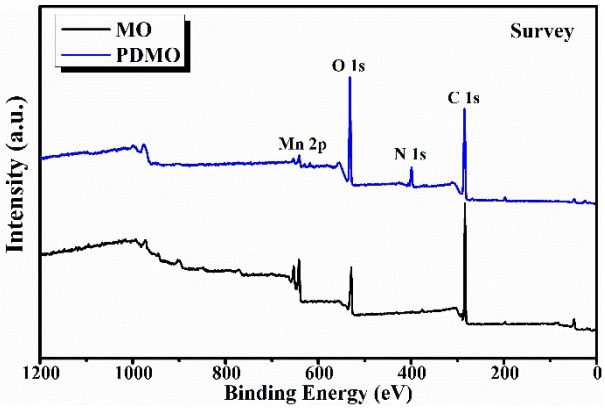

Figure S3 XPS survey of MO and PDMO samples.

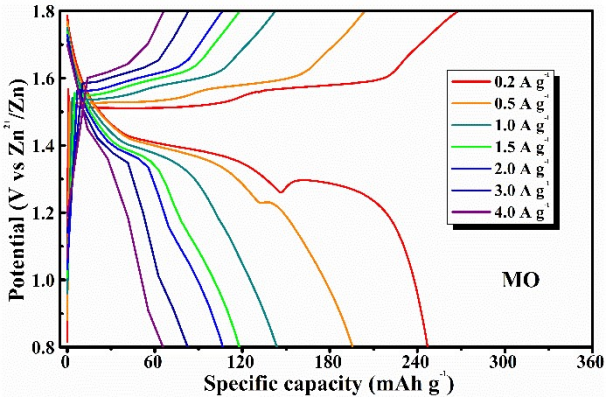

Figure S4 GCD curves of MO cathode at various current densities.

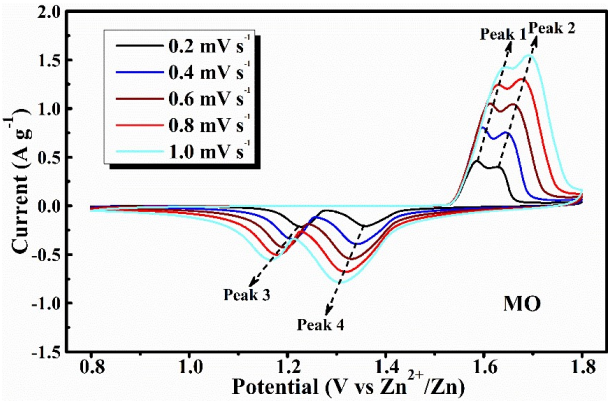

Figure S5 CV curves of MO cathode at various scan rates.

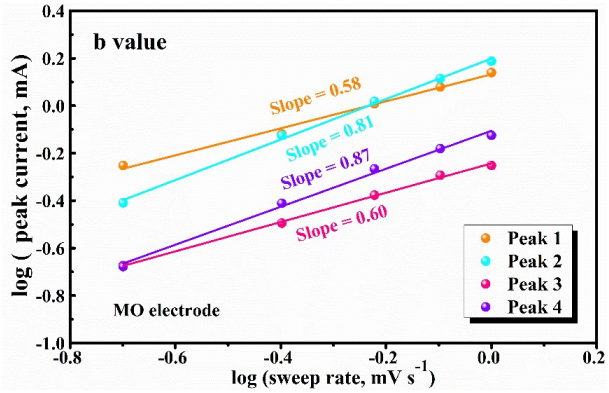

Figure S6 The fitting plots between log(*i*) and log(*v*) at various peak currents for MO cathode.

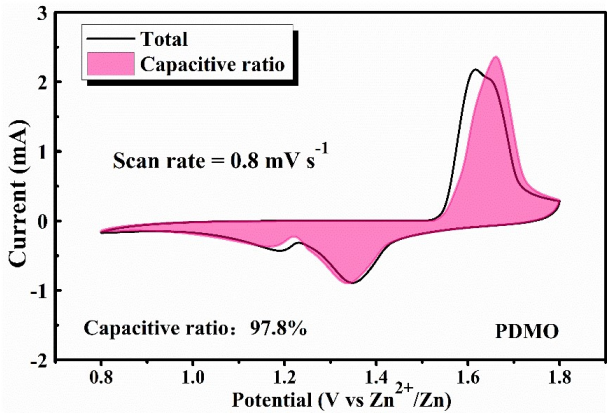

Figure S7 Capacitive contribution (pink region) of PDMO cathode at 0.8 mV s^{-1}.

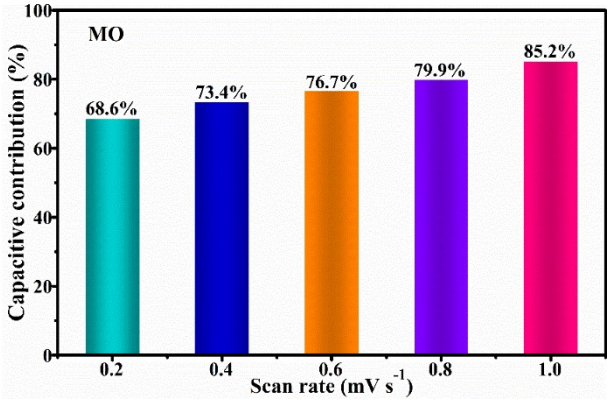

Figure S8 Capacitive contribution plots at different scan rates of MO cathode.

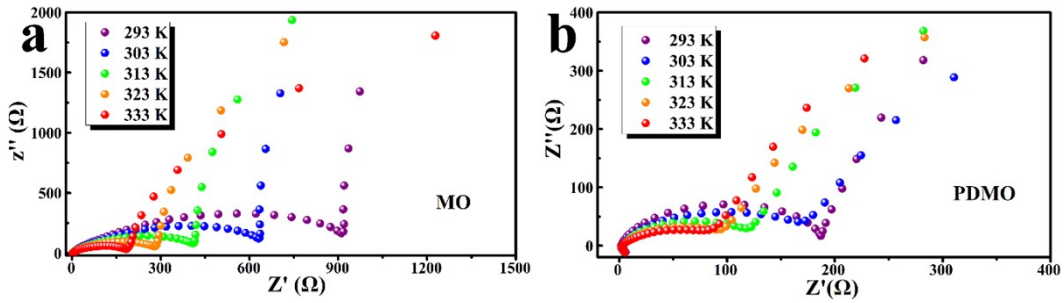

Figure S9 EIS spectra of MO and PDMO electrodes at various temperatures.

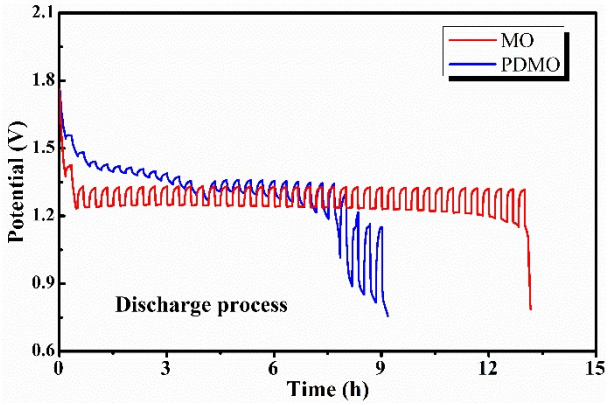

Figure S10 GITT curves of MO and PDMO cathode during the discharge process.

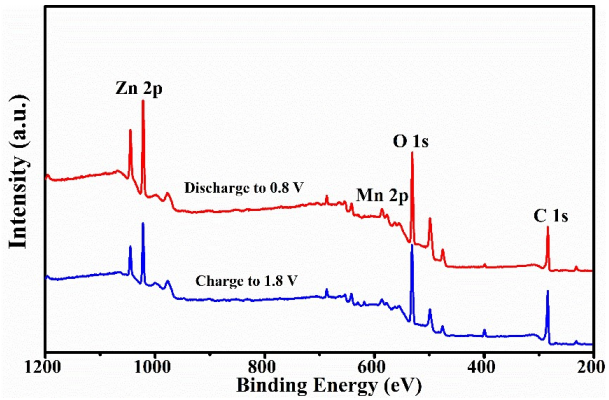

Figure S11 XPS survey spectra of PDMO cathode at the fully discharged and charged state.

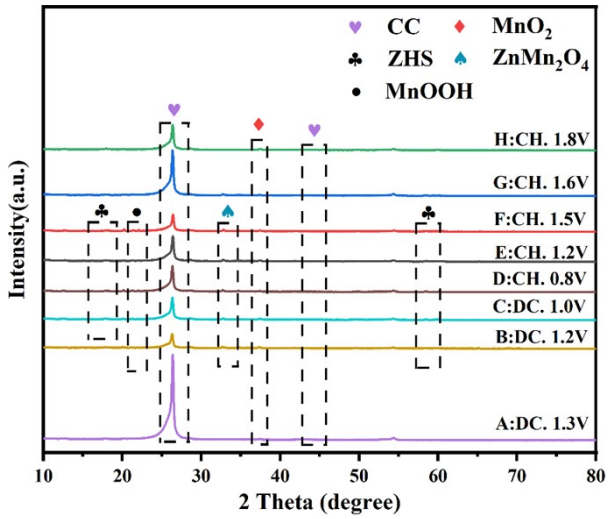

Figure S12 The *ex-situ* XRD patterns at different potentials of PDMO cathode

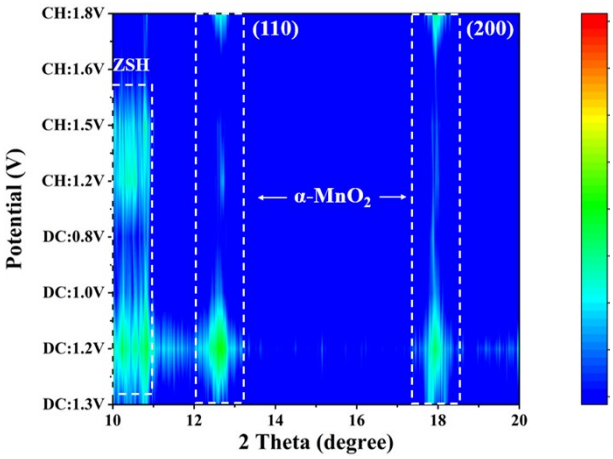

Figure S13 Contour mapping of *ex-situ* XRD patterns (10-20°) of PDMO at different voltages.

Table S1 Comparison of cycling performance PDMO cathode with previously reported Mn-based cathodes.

Mn-based Cathode types	Current density ($A\ g^{-1}$)	Cycling numbers	Final capacity ($mAh\ g^{-1}$)	Capacity retention (%)	Reference
PMC	1.0	500	152	72.7	5
MnO_2-birnessite	2.0	2000	134	79.6	9
Ca_2MnO_4	1.0	1000	100	80	10
$K_{0.21}MO$	2.0	1000	75	70	11
MNG-3	1.5	200	224.9	74.5	12
MOC-15	1.0	1500	60	40	13
β-MnO_2	0.2	1000	110	48.9	14
NM20	1.0	2500	115	85.6	15
ZMO QDs	1.0	1500	143.9	86.4	16
C@PODA/MnO_2	2,0	2000	138.4	89.3	17
PDMO	**2**	**3500**	**157**	**88.2**	**This work**

Reference:

1. G. Kresse and J. Hafner, *Phys. Rev. B*, 1993, **47**, 558-561.
2. P. E. Blöchl, *Phys. Rev. B*, 1994, **50**, 17953-17979.
3. W. Kohn and L. J. Sham, *Phys. Rev.*, 1965, **140**, A1133-A1138.
4. G. Kresse and J. Furthmüller, *Comp. Mater. Sci.,* 1996, **6**, 15-50.
5. Q. Gou, H. Luo, Y. Zheng, Q. Zhang, C. Li, J. Wang, O. Odunmbaku, J. Zheng, J. Xue, K. Sun and M. Li, *Small*, 2022, **18**, 2201732.
6. T. Wu, K. Zhu, C. Qin and K. Huang, *J. Mater. Chem. A*, 2019, **7**, 5612-5620.
7. T. Lu and F. Chen, *J. Comput. Chem*., 2012, **33**, 580-592.
8. J. Zhang and T. Lu, *Phys. Chem. Chem. Phys.,* 2021, **23**, 20323-20328.
9. N. Qiu, H. Chen, Z. Yang, S. Sun and Y. Wang, *Electrochim. Acta*, 2018, **272**, 154-160.
10. S. Guo, S. Liang, B. Zhang, G. Fang, D. Ma and J. Zhou, *ACS Nano*, 2019, **13**, 13456.
11. Y. Jiao, L. Kang, J. Berry-Gair, K. McColl, J. Li, H. Dong, H. Jiang, R. Wang, F. Corà, D. J. L. Brett, G. He and I. P. Parkin, *J. Mater. Chem. A*, 2020, **8**, 22075.
12. X. Zhang, J. Li, H. Ao, D. Liu, L. Shi, C. Wang, Y. Zhu and Y. Qian, *Energy Storage Mater.*, 2020, **30**, 337-345.
13. X. Chen, W. Li, Z. Zeng, D. Reed, X. Li and X. Liu, *Chem. Eng. J.*, 2021, **405**, 126969.
14. W. Liu, X. Zhang, Y. Huang, B. Jiang, Z. Chang, C. Xu and F. Kang, *J. Energy Chem.*, 2021, **56**, 365-373.
15. D. Zhang, J. Cao, X. Zhang, N. Insin, S. Wang, J. Han, Y. Zhao, J. Qin, Y. Huang, *Adv. Funct.Mater.,* 2021, **31**, 2009412.
16. S. Deng, Z. Tie, F. Yue, H. Cao, M. Yao, Z. Niu, *Angew. Chem. Int. Ed.*, 2022, **61**, 2115877.
17. Y. Zhao, R. Zhou, Z. Song, X. Zhang, T. Zhang, A. Zhou, F. Wu, R. Chen and L. Li, *Angew. Chem. Int. Ed.*, 2022, **61**, 2212231.